Adsorption characteristics and mechanism of tetracycline by nitrogen-rich porous carbon material derived from peony seed shell

Qiong Liu*, Yuhan Xu, Xinghang Li

School of Environmental Engineering and Chemistry, Luoyang Institute of Science and Technology, No. 90 of Wangcheng Road, Luoyang 471000, China, email: heidy2007@126.com (Q. Liu)

ABSTRACT

Nitrogen-rich porous carbon (NPC) material was prepared from peony seed shell by one-step pyrolysis, and the physicochemical properties were characterized. The results showed that the as-prepared material had high surface area (3,509.1 $m^2 \cdot g^{-1}$) and abundant functional groups containing nitrogen and oxygen. The NPC material displayed excellent adsorption capacity (q_e = 750 $mg \cdot g^{-1}$) for tetracycline (TC) even at pH = 3~11 or in the presence of salt ions ($C_{Na_2SO_4/NaCl}$ = 0.1 ~ 0.5 mol L^{-1}). With Langmuir and pseudo-second-order models, the adsorption process of being spontaneous and endothermic could be satisfactorily described and the adsorption capability was derived to be about 892.7 $mg \cdot g^{-1}$ at 25°C. The saturated NPC was regenerated by pyrolysis technology and used in the treatment of TC simulated wastewater. After 4 cycles, the adsorption amount of TC on NPC still remained above 500 $mg \cdot g^{-1}$. Combined with the characterization analysis, it could be inferred that the adsorption of TC by NPC benefited from the high specific surface area and hierarchical pore structure of NPC, in addition to the active groups such as carbonyl, graphite-nitrogen and sp^2 carbon on its surface.

Keywords: Peony seed shell derived carbon; Adsorption; Tetracycline; Mechanism

1. Introduction

Tetracycline (TC) is a broad-spectrum antibiotic applied in clinical medicine, veterinary medicine and feed additives. Recently, the TC pollution has attracted many domestic and foreign researchers [1,2]. Various approaches have been adopted to remove TC in the environment, including advanced oxidation, membrane separation, electrochemical methods and adsorption [3,4]. Among them, adsorption has been brought into focus owing to its low-cost, high efficiency and simple operation [5].

The core task of adsorption is to design and develop the adsorbent. Different from the adsorption materials like zeolite, resin and clay, biochar deserves great attention as its simple fabrication, a wealth of porous structure and surface functional groups [6,7]. However, there is a large variation in the adsorption quantity of different precursor materials such as rice waste, *Suaeda salsa* and walnut shell, ranging from 70.17 to 607.00 $mg \cdot g^{-1}$ [8–11]. Therefore, the reasonable selection of precursor materials is crucial to improve the adsorption quantity of TC on biochars.

Peony seed shell (PS) is a by-product of peony seed oil extraction. The lack of related technologies including processing and utilization results in the resource waste and environment pollution [12]. Previous studies have found that PS not only has a highly ordered three-dimensional structure, but also contains a variety of bioactive components such as fatty acids, polysaccharides, polyphenols and flavonoids [13]. During the pyrolysis process, the unique structure can serve as the natural template for the pore formation, while the active ingredients provide the possibility for the occurrence of chemical reactions. At present, PS-derived

---

* Corresponding author.

carbons have achieved in the removal of dyes, heavy metals and other pollutants in water [14–16]. Nevertheless, these studies are still unable to expatiate the essential relation between the surface chemistry and structural characteristics of adsorbents and the removal of pollutants, which is essential to further improve the removal efficiency and expand the applications.

In this paper, nitrogen-rich porous carbon (NPC) derived from peony seed shell was prepared by one-step pyrolysis. The underlying mechanisms were revealed by analyzing the composition and structural properties of NPC material, as well as its adsorption behavior to TC. This study could be expected to provide a certain reference for the reutilization of biomass wastes and remediation of TC pollution in water.

2. Materials and methods

2.1. Reagents and materials

TC (USP, 99% in purity) was purchased from Aladdin Reagent Co., Ltd. Hydrochloric acid (HCl, 36%~38%), sodium hydroxide (NaOH, ≥98%), potassium hydroxide (KOH, 95%), sodium chloride (NaCl, ≥99.5%), sodium sulfate (Na$_2$SO$_4$, ≥99.5%) and melamine (C$_3$H$_6$N$_6$, 99%) were all analytical reagents and obtained from Tianjin Kemiou Chemical Reagent Co., Ltd. The PS was obtained from Luoyang National Garden (Henan Province, PR China).

2.2. Preparation of NPC

Prior to use, the PS was rinsed, dried and ground to the desired particle size (40–25 mesh). The preparation procedures of NPC could be described as follow. Firstly, the treated PS (12.0 g) was placed into a 250 mL conical flask with 90 mL of 10 wt.% KOH solution and stirred at 80°C for 1 h. After adding 8.4 g of melamine, the mixture was stirred for another 1 h and then transferred into a drying oven for 48 h at 80°C to evaporate water. Subsequently, the resulting material was annealed at 800°C for 3 h in the presence of nitrogen with a heating velocity of 2°C·min^{-1}. Finally, the carbonized product was washed with 15 wt.% HCl solution and distilled water alternately (until pH ≈ 7) before dried at 80°C overnight.

2.3. Characterization of TC and NPC

The surface morphology was investigated by the field-emission scanning electron microscope (FE-SEM, Gemini 300, ZEISS) and transmission electron microscopy (FE-TEM, JEM-F200, JEOL). The crystalline state was analyzed using X-ray diffraction (XRD, D8 Advance, Bruker) with Cu Kα radiation. Raman spectroscopy (LabRAM HR Evolution, Horiba) were employed to analyze the carbon defects and graphitization. Porous structure was determined using a surface and porosity analyzer (Autosorb iQ3, Quantachrome). The functional groups were identified by Fourier-transform infrared spectroscopy (FTIR, Nexus-470, Nicolet) and X-ray photoelectron spectroscopy (XPS, Thermo Scientific K-Alpha, Thermo Fisher) was performed with a monochromatic Al Kα source to detect the chemical states.

2.4. Adsorption experiments

Adsorption experiments were conducted by mixing 12.5 mg of NPC with 50 mL of TCs solution in the stopped conical flask. The flask was shaken in a thermostatic oscillator at the speed of 160 rmp. After the predefined time interval, the solution was filtered and analyzed for the concentration of TCs using UV-Vis Spectrophotometer. The influence of initial pH (3.0–11.0), ionic strength (0.1–0.5 mol·L^{-1} of NaCl or Na$_2$SO$_4$), TC concentration (50–400 mg·L^{-1}), adsorption time (0–690 min), and temperature (15°C, 20°C, 25°C, 35°C and 45°C) on adsorption was also investigated. Solution pH was adjusted with 0.1 mol·L^{-1} HCl and 0.1 mol·L^{-1} NaOH. The adsorption quantity (q) was determined by Eq. (1):

$$q = \frac{\left(C_0 - C_e\right)V}{W} \tag{1}$$

where V, C_0 and C_e each denote the volume (L), concentration (mg·L^{-1}) at initial and equilibrium stages of TC solution, and W stands for the quantity of NPC.

All the data were the average of three independent runs and all the results were reproducible with ±5% error limit.

2.5. Desorption and reusability studies

The regeneration was performed by the pyrolysis of NPC adsorbed by TC at 700°C for 1 h. The regenerated NPC was directly deployed in the next adsorption cycle. After the equilibrium was attained, the adsorbent was collected with filters and the residual TC was determined. The reusability procedures were carried out for four times.

3. Results and discussion

3.1. Characterization of TC and NPC

3.1.1. Scanning electron microscopy and transmission electron microscopy analysis

Fig. 1a shows that PS is a three-dimensional layered structure. After carbonization, a significant number of defects and channels could be observed clearly due to the full opening of the pores. (Fig. 1b–d), which was critical for the exposure of active sites on the surface of NPC and the transport of TC [17].

3.1.2. Nitrogen adsorption and desorption

The nitrogen adsorption and desorption isotherm of NPC is displayed in Fig. 2a. The curve obviously conformed to the characteristics of type IV isotherm. The relative pressure P/P_0 was between 0.4 and 0.9 with H$_4$ hysteresis ring, indicating that there were a mass of mesopores in NPC. When P/P_0 was less than 0.1, the sharp increase of isotherm demonstrated the massive existence of micropores in the material. When $P/P_0 > 0.9$, the increasing tendency of adsorption curve implied the presence of large pores. In summary, the multistage pore structure of NPC, which coincided with the pore diameter distribution curve (Fig. 2b), provided the favorable conditions for TC adsorption [18–20].
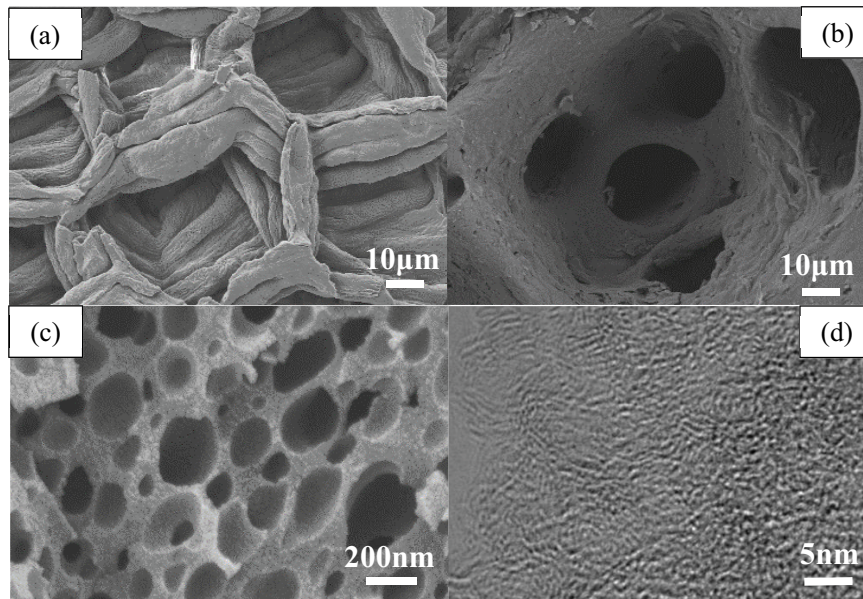
Fig. 1. Scanning electron microscopy images of PSC (a) and nitrogen-rich porous carbon (b), transmission electron microscopy (c) and high-resolution transmission electron microscopy (d) images of nitrogen-rich porous carbon.
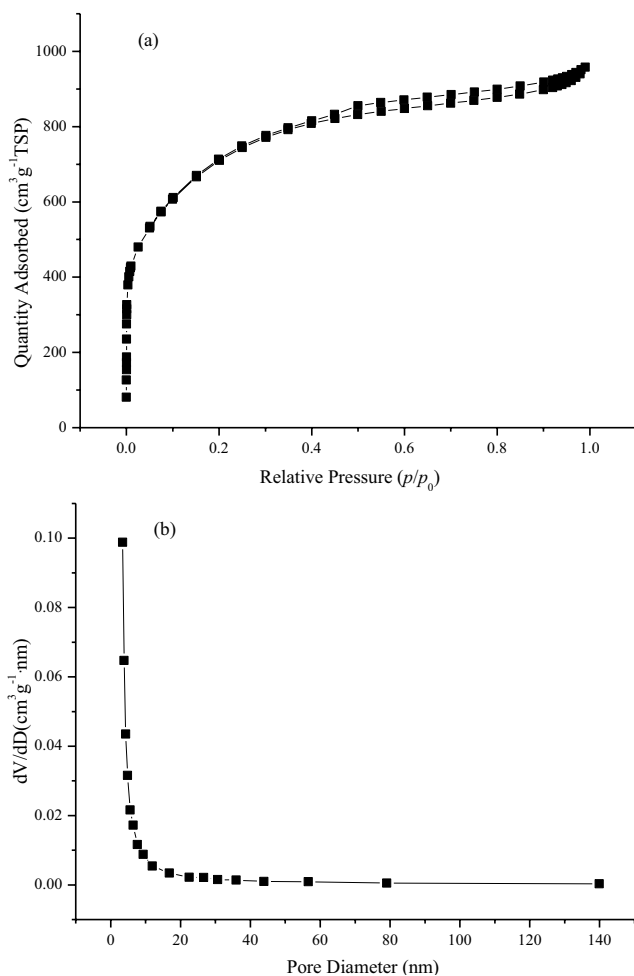

Fig. 2. Nitrogen adsorption and desorption curves (a) and pore-size distribution (b) of nitrogen-rich porous carbon.

3.1.3. XRD analysis

As illustrated in Fig. 3a, the XRD pattern showed a pair of wide diffraction peaks near $2\theta = 22.3°$ and $43.2°$, representing the (002) and (100) planes of amorphous and crystalline carbon, respectively. Among them, the peak intensity of (100) crystal face reflected the degree of graphitization of the material [21]. Fig. 3b shows the Raman spectra of NPC and two diffraction peaks appeared near 1,341 and 1,583 cm^{-1}, which belonged to peak D and peak G, respectively. The ratio of two strengths (I_D/I_G) was applied to reveal the defect level in the carbon layer [22,23]. The I_D/I_G value of 1.09 confirmed the existence of defects and distortion, which could be caused by N-doping on the surface of NPC [24].

3.1.4. XPS analysis

For further understanding the chemical properties of material surface, the XPS spectroscopy was employed and illustrated in Fig. 4. As seen from Fig. 4a, the NPC were mainly composed of carbon, oxygen and nitrogen, appearing in C1s (284.8 eV), O1s (532.1 eV) and N1s (401.9 eV), respectively. The spectrum of C1s (Fig. 4b) could be fitted to three peaks, namely C=C/C–C (284.8 eV), C=O (286.0 eV) and π–π^* (290.2 eV), while the three peaks of N1s (Fig. 4c) could be ascribed to pyridine nitrogen (398.9 eV), pyrrole nitrogen (400.0 eV) and graphite nitrogen (401.9 eV). Moreover, the O1s spectrum was decomposed into two peaks: C=O (531.9 eV) and C–OH/C–O–C (532.8 eV) (Fig. 4d). To sum up, the surface of NPC contained abundant functional groups, which provided favorable conditions for the adsorption of TC [25].

3.2. Batch adsorption

3.2.1. Adsorption kinetics

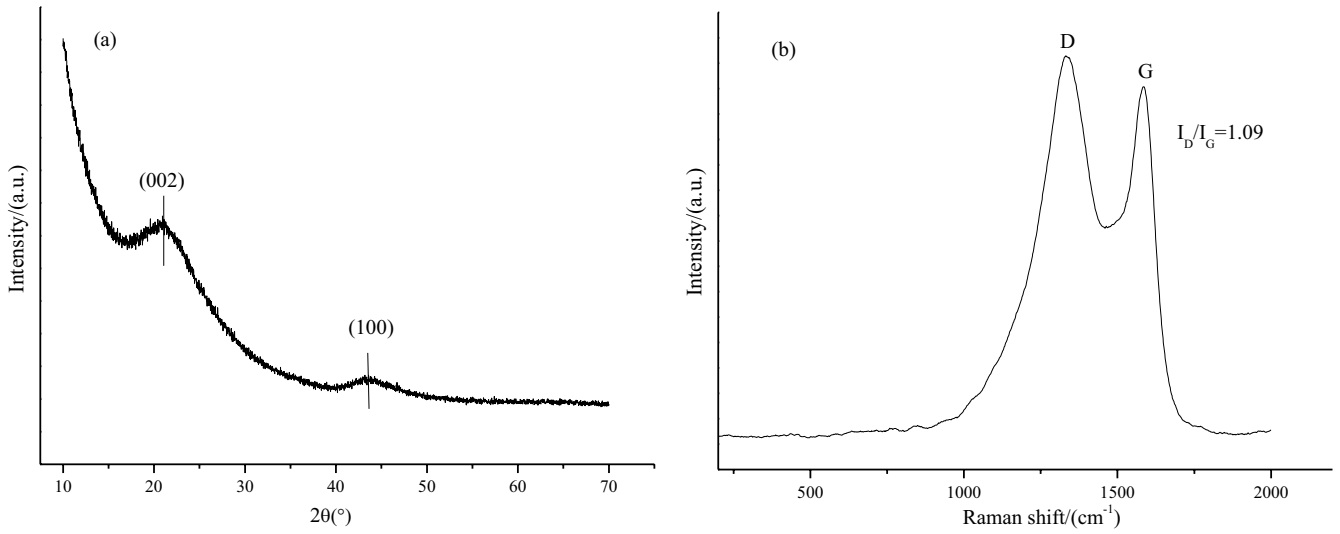To investigate the kinetics of TC adsorption by NPC, pseudo-first-order, pseudo-second-order, Elovich and

Fig. 3. X-ray diffraction pattern (a) and Raman spectroscopy (b) of nitrogen-rich porous carbon.
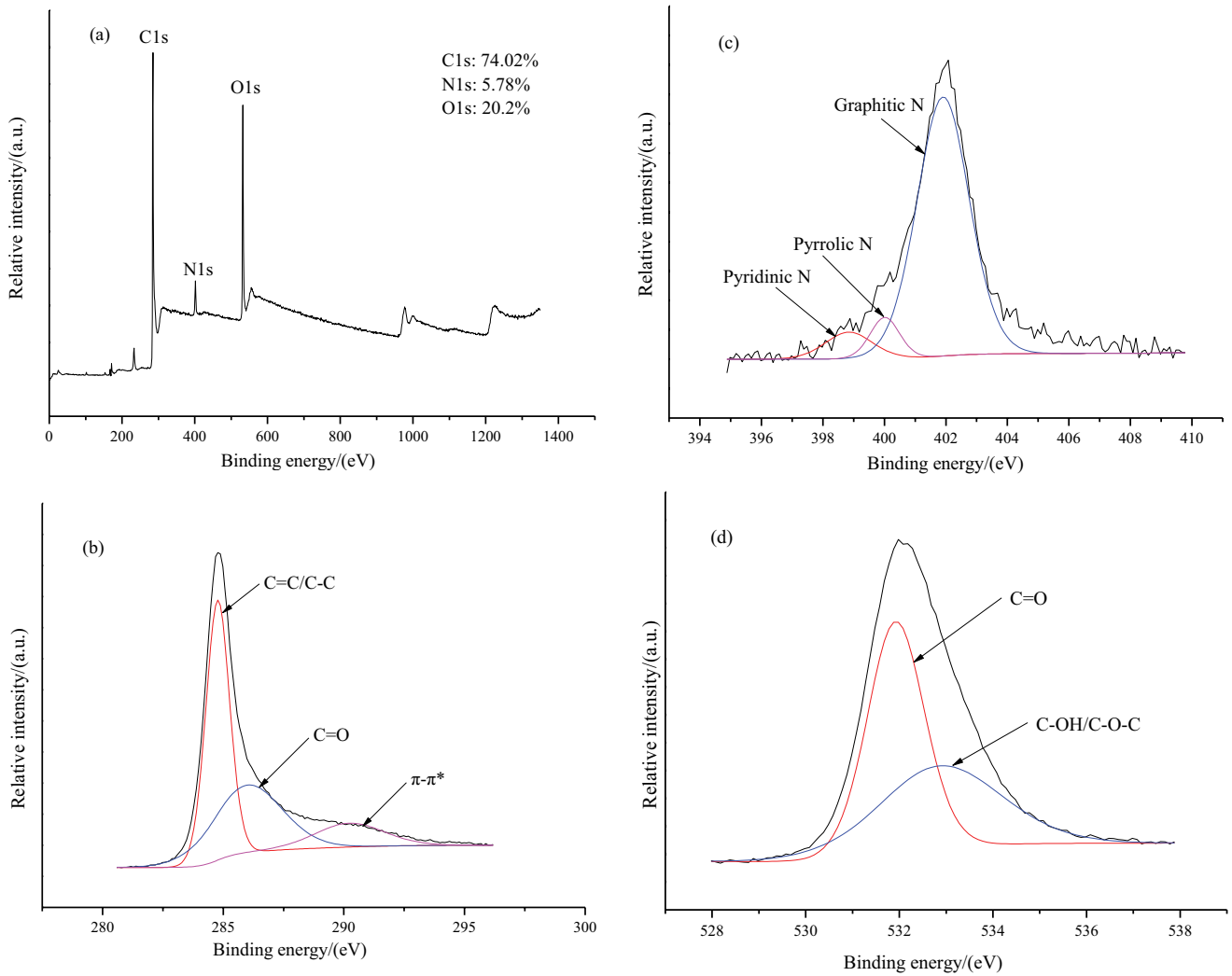

Fig. 4. X-ray photoelectron spectroscopy survey (a), high-resolution C1s (b), N1s (c) and O1s (d) of nitrogen-rich porous carbon.

intraparticle diffusion models (Table 1) were selected and the results are demonstrated in Fig. 5 and Table 2. With the extension of time, as seen from Fig. 5a, the adsorbed TC amount (q_t) presented a "fast before slow" growth trend and the adsorption equilibrium reached within 12 h. In addition,

the TC adsorption remarkably increased with the temperature, indicative of endothermic nature of the process.

On observing Table 2 it was found that pseudo-second-order model fitted the data for TC adsorption better ($R^2 > 0.995$, $\Delta q_e < 0.002\%$). This implied that chemisorption

Table 1
Formulas and parameters of kinetic and isotherm models

| Model	Expression	Parameter
Pseudo-first-order model	$q_t = q_e \left[1 - \exp\left(-k_1 t\right) \right]$	q_t (mg·g^{-1}) is the adsorption quantity at time (t); k_1 (g·mg^{-1}·min^{-1}) is the rate constant of equation.
Pseudo-second-order model	$q_t = \dfrac{k_2 q_e^2 t}{\left(1 + k_2 q_e t\right)}$	k_2 (g·mg^{-1}·min^{-1}) is the rate constant of equation.
Elovich equation	$q_t = \dfrac{1}{\beta} \ln\left(\alpha\beta\right) + \dfrac{1}{\beta} \ln t$	α (g·mg^{-1}·min^{-1}) is the initial adsorption rate constant; β (g·mg^{-1}) is related to the extent of surface coverage and activation energy for chemisorption.
Intraparticle diffusion model	$q_t = k_d t^{0.5} + C$	k_d is intraparticle diffusion rate constant and C is the intercept.
Langmuir model	$q_e = \dfrac{q_m K_L C_e}{1 + K_L C_e}$	q_m (mg·g^{-1}) is the saturated adsorption amount; K_L (L·mg^{-1}) is the constant related to the binding energy.
Freundlich model	$q_e = K_F C_e^{1/n_F}$	K_F and n_F are Freundlich constants.
Dubinin–Radushkevich model	$q_e = q_m \exp\left(-k_{DR} \varepsilon^2\right)$ $\varepsilon = RT \ln\left(1 + \dfrac{1}{C_e}\right)$ $E = \dfrac{1}{\sqrt{2 k_{DR}}}$	k_{DR} is Dubinin–Radushkevich constant; ε is the Polanyi potential; R is universal gas constant (8.314 J·K^{-1}·mol^{-1}); T (K) is temperature; E (kJ·mol^{-1}) is the adsorption mean free energy.
Temkin model	$q_e = \dfrac{RT}{b} \ln\left(A_T C_e\right)$	A_T (mL·mg^{-1}) is the model constant; b (J·mol^{-1}) is a constant related to heat of sorption.
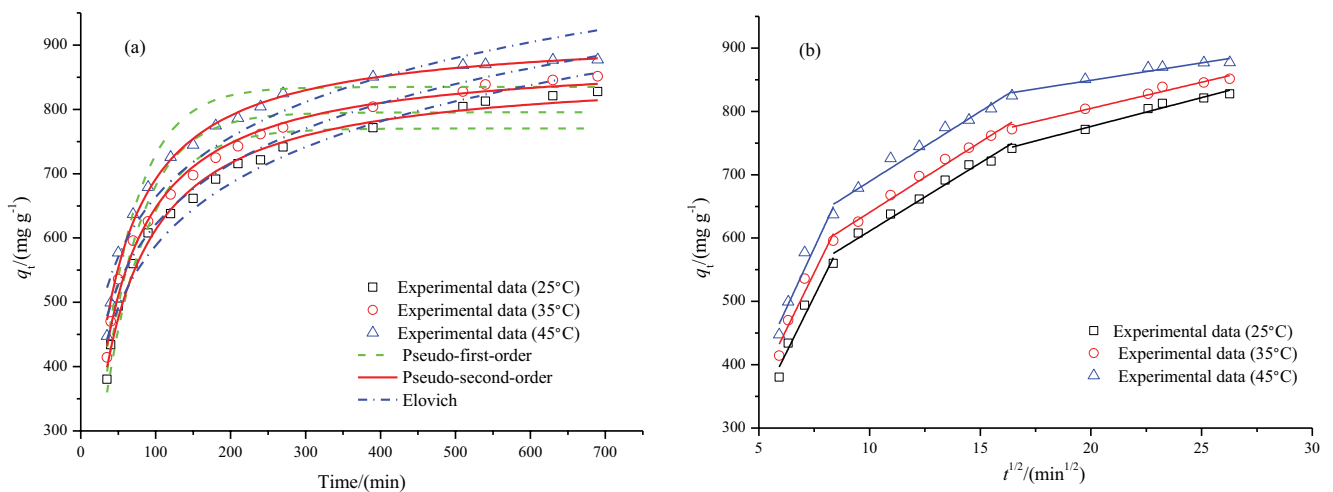
Fig. 5. Non-linear fits of pseudo-first-order, pseudo-second-order and Elovich kinetic models (a) and linear fit of intraparticle diffusion model (b) for the tetracycline adsorption at 25°C, 35°C and 45°C (adsorbent dose: 0.4 g·L^{-1}, initial concentration: 250 mg·L^{-1}, pH: 3.5).

Table 2
Kinetic parameters for tetracycline adsorbed onto nitrogen-rich porous carbon

Models	Parameters	Temperature (°C)		
		25	35	45
Pseudo-first-order	k_1 (min^{-1})	0.0180	0.0194	0.0207
	q_e (mg·g^{-1})	770.3	795.4	834.9
	R^2	0.916	0.909	0.933
	Δq_e (%)	0.070	0.068	0.055
Pseudo-second-order	k_2 (g·mg^{-1}·min^{-1})	2.85×10^{-5}	3.09×10^{-5}	3.26×10^{-5}
	q_e (mg·g^{-1})	862.3	884.2	921.7
	R^2	0.996	0.997	0.999
	Δq_e (%)	0.0017	0.0015	0.0013
Elovich	α (mg·g^{-1}·min^{-1})	95.553	132.184	188.085
	β (g·mg^{-1})	0.0072	0.0074	0.0075
	R^2	0.963	0.960	0.933
	Δq_e (%)	0.062	0.059	0.068
Intraparticle diffusion	K_{id1} (mg·g^{-1}·min$^{-0.5}$)	70.478	71.326	75.563
Stage 1	C_1 (mg·g^{-1})	−20.610	10.437	17.455
	R^2	0.942	0.921	0.921
Stage 2	K_{id2} (mg·g^{-1}·min$^{-0.5}$)	21.529	22.176	22.079
	C_2 (mg·g^{-1})	395.659	418.763	468.615
	R^2	0.985	0.991	0.981
Stage 3	K_{id3} (mg·g^{-1}·min$^{-0.5}$)	9.119	8.271	5.494
	C_3 (mg·g^{-1})	593.798	693.312	739.276
	R^2	0.973	0.975	0.932

Notes: $\Delta q_e\left(\%\right)=100\sqrt{\dfrac{\sum\left[\left(Q_{e,n}-Q_{m,n}\right)/Q_{e,n}\right]^2}{n-1}}$, $Q_{e,n}$ and $Q_{m,n}$ (mg·g^{-1}) are the adsorption amount of experiment and calculation, respectively, and n is the number of observation.

predominated in the whole process, which was consistent with the TC adsorption by corn stalk-based biochar using KOH as activator [26,27]. Given the importance of diffusibility for the overall velocity of adsorption, the intraparticle diffusion model was applied as the complement to above models. As shown in Fig. 5b, the intraparticle diffusion regulated the sorption rate with boundary layer diffusion by TC concentration, reaction temperature and the accessibility of active site on NPC. What followed was the slow diffusion of TC from larger pores to micropores until the equilibrium was finally achieved. The middle part of curve didn't pass through the origin, implying that the adsorption was jointly controlled by intraparticle diffusion and film diffusion [28].

3.2.2. Adsorption isotherms

The determination of adsorption isotherm was of great significance for further study on the surface properties of adsorbent and inference of adsorption mechanism. The adsorption experiment of TC solution with different concentrations by NPC was performed and the data was fitted by the isotherm models (Table 1) of Langmuir, Freundlich, Dubinin–Radushkevich and Temkin. When increasing the TC concentration, the adsorption amount (q_e) of NPC from Fig. 6 could be seen increasing rapidly at first and then gradually levelling off, which was relevant to the occupation

and saturation of active sites. Furthermore, the increase of q_e value with temperature demonstrated that the adsorption could benefit from the higher temperature, which was in accordance with the results of kinetic studies [29].

As described in Table 3, Langmuir model fitted the adsorption of TC by NPC best, considering its high coefficients ($R^2 > 0.980$) and low error values ($\Delta q_e < 0.0291\%$) as well as the correspondence between simulated value (q_m) and measured value (q_e) at different temperatures. Moreover, the increase of model constant (K_L) with temperature manifested that the adsorption affinity of NPC for TC was enhanced by increasing the temperature [33]. The maximum monolayer adsorption amounts of TC on NPC was 892.7 mg·g^{-1} at 25°C. Compared with other adsorbents in the published literature (Table 4), the NPC material exhibited great advantage in TC adsorption.

The Temkin model wasn't suitable for describing the adsorption process in view of the lower R^2 and higher Δq_e values. In contrast, Dubinin–Radushkevich model had better fitting performance. The apparent free energy of adsorption was calculated to be about 4.71 kJ·mol^{-1} ($1 < E < 8$ kJ·mol^{-1}), confirming the nature of physical adsorption.

3.2.3. Adsorption thermodynamics

Thermodynamic parameters including enthalpy change ($\Delta H°$), Gibbs free energy change ($\Delta G°$) and entropy change

($\Delta S°$) were calculated based on the adsorption isotherms at different temperatures. As shown in Table 5, the negative $\Delta G°$ meant that the adsorption reaction spontaneously occurred. Moreover, the $\Delta G°$ (absolute values) increased with temperature, signifying that the spontaneous trend was larger at higher temperature. The positive $\Delta H°$ suggested the adsorption was endothermic, that is, increasing

the temperature was conducive to the adsorption. The $\Delta H°$ value less than 40 kJ·mol⁻¹ illustrated the presence of physical adsorption, which coincided with the apparent activation energy (E_a) being between 5 and 40 kJ·mol⁻¹. The positive $\Delta S°$ revealed that the adsorption of NPC for TC increased the randomness of solid–liquid interface.

3.3. Adsorption mechanisms

3.3.1. Electrostatic interaction and pore-filling effect

In order to clarify the role of electrostatic interaction in the adsorption of TC by NPC, the effect of initial pH was investigated and the result is shown in Fig. 7a. When the pH increasing from 3.0 to 7.0, the adsorption amount (q_t) only dropped 2%. Further raising to 11, the q_t value decreased by 19%. For one thing, as an amphiphilic compound, TC could exist in the form of cations (TCH³⁺), zwitterions (TCH²⁺) and anions (TCH²⁻) in aqueous solution [37]. With increasing the pH, TC gradually shifted from cation to anion. On arriving at the isoelectric point of NPC (pH$_{pzc}$ = 8.0), the interaction between TC and NPC shifted from weak electrostatic attraction to strong electrostatic repulsion. For another, the increased pH promoted the deprotonation of the amino and phenolic hydroxyl groups on the surface of TC and inhibited the possible π–π and cation-π electron donor–acceptor (EDA) interaction between TC and the graphitized structure of NPC, thus further reducing the adsorption quantity [38]. Even under alkaline condition, the adsorption amount of NPC for TC still retained above 750.48 mg·g⁻¹, indicating that electrostatic action was not the predominant mechanism
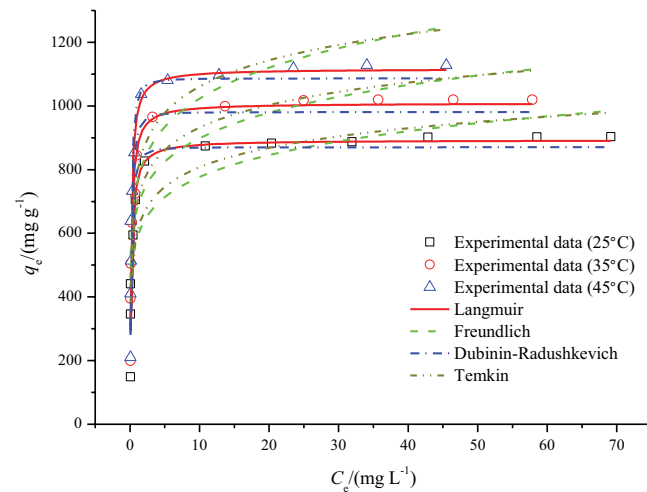
Fig. 6. Non-linear fits of Langmuir, Freundlich, Dubinin–Radushkevich and Temkin isotherm models for the tetracycline adsorption at 25°C, 35°C and 45°C (adsorbent dose: 0.25 g·L⁻¹, contact time: 12 h, pH: 3.5).

Table 3
Isotherm parameters for tetracycline adsorbed onto nitrogen-rich porous carbon

Models	Parameters	Temperature (K)		
		298	308	318
Langmuir	K_L (L·mg⁻¹)	5.687	5.994	6.541
	q_m (mg·g⁻¹)	892.7	1008.9	1116.6
	q_e (mg·g⁻¹)	903.1	1019.8	1128.6
	R^2	0.980	0.992	0.993
	Δq_e (%)	0.0291	0.0187	0.0192
Freundlich	K_F (mg·g⁻¹ (L·mg⁻¹)$^{1/n}$)	586.1	676.8	756.8
	$1/n$	0.122	0.123	0.131
	R^2	0.757	0.776	0.768
	Δq_e (%)	0.589	0.458	0.475
Dubinin–Radushkevich	k_{DR}	2.79×10^{-8}	2.53×10^{-8}	2.26×10^{-8}
	q_m (mg·g⁻¹)	870.3	980.7	1086.6
	R^2	0.915	0.932	0.939
	Δq_e (%)	0.0294	0.0183	0.0182
Temkin	A_T	898.3	937.2	743.1
	b	27.94	25.12	22.21
	R^2	0.828	0.850	0.845
	Δq_e (%)	0.484	0.363	0.370

Notes: $\Delta q_e \left(\% \right) = 100 \sqrt{\dfrac{\sum \left[\left(Q_{e,n} - Q_{m,n} \right) / Q_{e,n} \right]^2}{n-1}}$, $Q_{e,n}$ and $Q_{m,n}$ (mg·g⁻¹) are the adsorption amount of experiment and calculation, respectively, and n is the number of observation.

Table 4
Comparison of adsorption capacities of various adsorbents for tetracycline at 25°C

Feedstock	Modifier	Pyrolysis temperature (°C)	Tetracycline concentration (mg·L^{-1})	Adsorbent dose (g·L^{-1})	Q_{max} (mg·g^{-1})
PS [This study]	Melamine	800	20~400	0.4	892.7
Lotus seed [30]	$K_2C_2O_4$/$CaCO_3$	800	20~160	0.1	506.6
Wheat straw [31]	KOH/$KMnO_4$	700	10~200	0.25	542.4
Tea waste [32]	$KHCO_3$	700	10~200	0.5	425.17
Wheat straw [5]	$FeCl_3$/$CO(NH_2)_2$	700	10~200	1.0	156
Zeolite [34]	CTAB	–	100	1.5	7.0
Pyrrole [35]	$FeCl_3$	–	100	0.6	5.0
Maize stalks [36]	–	–	100	2.5	7.0

Table 5
Thermodynamic parameters for tetracycline adsorbed onto nitrogen-rich porous carbon

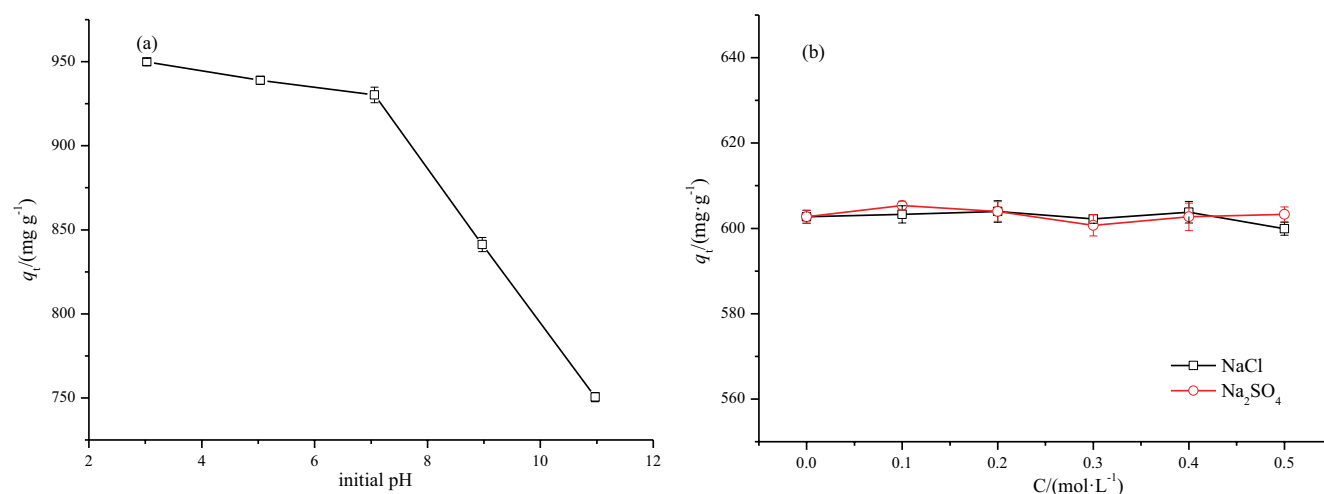| E_a (kJ·mol^{-1})	$\Delta H°$ (kJ·mol^{-1})	$\Delta S°$ (J·mol^{-1}·K^{-1})	$\Delta G°$ (kJ·mol^{-1})				
			288 K	293 K	298 K	308 K	318 K
5.33	5.49	0.142	−35.4	−36.1	−36.7	−38.1	−39.6

Fig. 7. Effect of ionic strength (a) and solution pH (b) on the adsorption of tetracycline (adsorbent dose: 0.4 g·L^{-1}, initial concentration: 250 mg·L^{-1}, temperature: 25°C, contact time: 12 h).

[23,39]. This could be confirmed by the slight influence of ionic strength on the adsorption (Fig. 7b).

Wang et al. [40] believed that pore-filling played a pivotal role in the adsorption of organic pollutants based on the unique physical characteristics of biochars. The Brunauer–Emmett–Teller (BET) results suggested that the specific surface area (S_{BET}), total pore volume (V_{total}) and micropore volume (V_{micro}) were reduced by 80%, 74% and 65%, respectively after adsorption, and average pore size (D_p) dropped from 2.350 to 0.581 nm (Table 6). Obviously, the pore-filling was instrumental in adsorption of TC by NPC. This could be demonstrated by the positive correlation of the S_{BET}, V_{total} with q_e (Fig. 8). Overall, the presence of microporous and mesoporous structure in NPC was unquestionably beneficial to the adsorption of TC [41–43].

Table 6
Brunauer–Emmett–Teller results of the nitrogen-rich porous carbon before and after tetracycline adsorption

Nitrogen-rich porous carbon	S_{BET} (m^2·g^{-1})	V_{total} (cm^3·g^{-1})	V_{micro} (cm^3·g^{-1})	D_p (nm)
Before adsorption	3,509.1	1.335	1.035	2.225
After adsorption	522.8	0.384	0.361	0.581

3.3.2. π–π and n–π EDA interactions

In addition to the physical structure, the chemical properties of adsorbent were crucial to the adsorption of organic pollutants. To further reveal the adsorption mechanism of
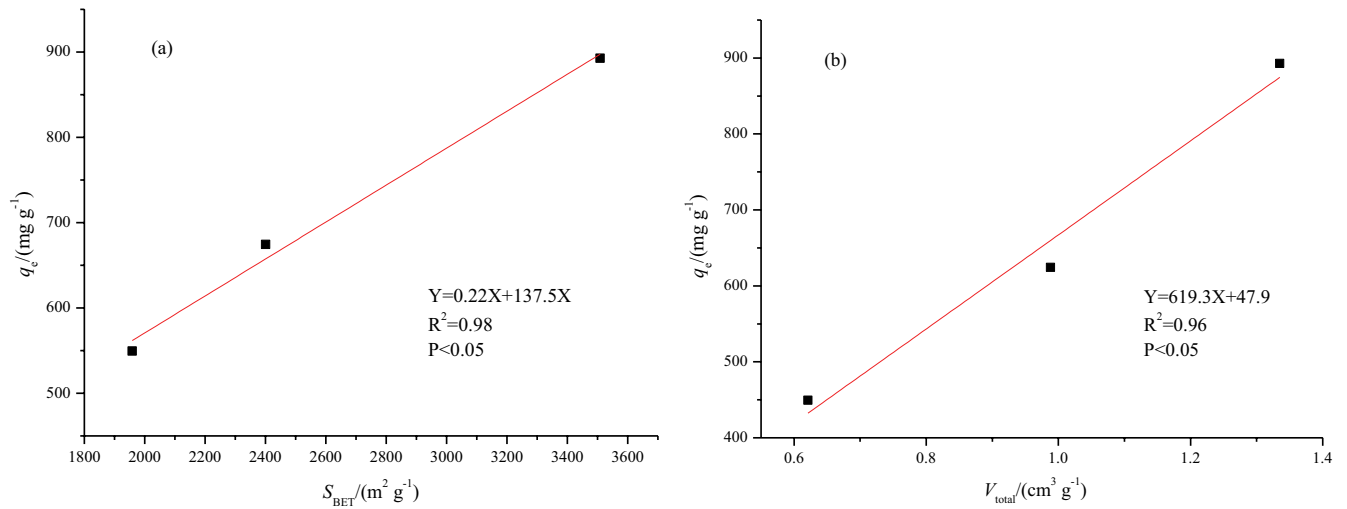
Fig. 8. Correlation between adsorption amount (q_e) and the properties of nitrogen-rich porous carbon. S_{BET} (a) and V_{total} (b).
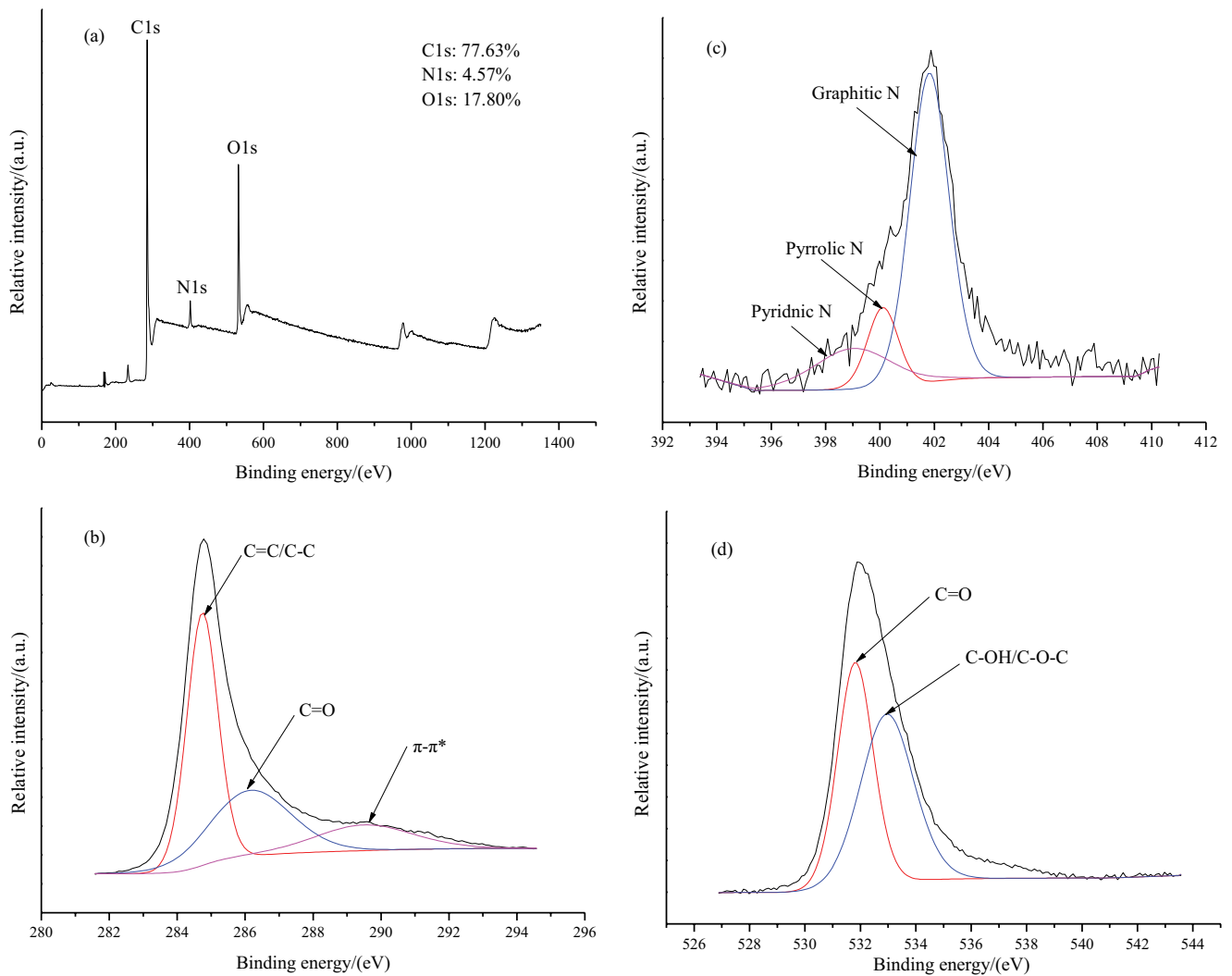

Fig. 9. X-ray photoelectron spectroscopy survey (a), high-resolution C1s (b), N1s (c) and O1s (d) of nitrogen-rich porous carbon after adsorption.

TC by NPC, the XPS analysis was conducted and the results are displayed in Fig. 9. Compared with before adsorption (Fig. 4), there was obvious difference in the composition content and binding energy. In particular, the binding energy of $\pi-\pi^*$ shifted and the content of graphitic nitrogen was reduced markedly, implying that the corresponding functional groups participated in the adsorption. As known, the structure of TC molecule contained phenolic, amino, enol, ketone and other polar functional groups, which have strong electron-attractive ability and could produce relatively strong interaction of $\pi-\pi$ electrons with aromatic rings or unsaturated structures on NPC [44]. In addition, the significant decrease in C=O content might be associated with $n-\pi$ EDA interaction between NPC and benzene ring of TC [45]. These conclusions were in complete conformity to those obtained from the FTIR spectra of NPC after adsorption/desorption of TC (Fig. 10).

The pore-filling effect, $\pi-\pi/n-\pi$ EDA and cation-π interaction could contribute to the adsorption of TC on NPC (Fig. 11).
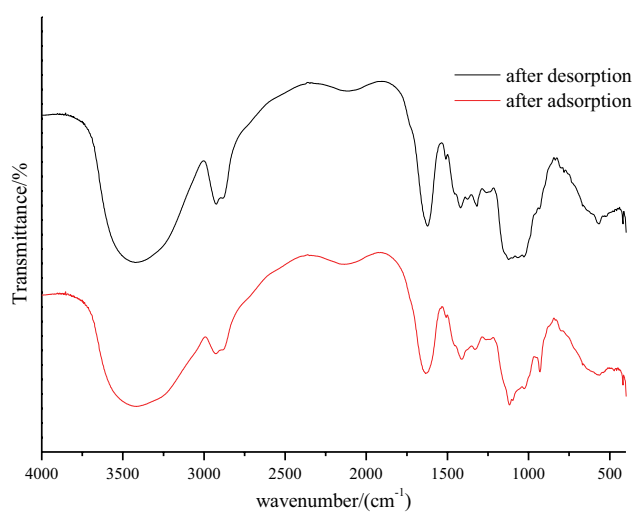

Fig. 10. Fourier-transform infrared spectra of nitrogen-rich porous carbon after adsorption/desorption of tetracycline.
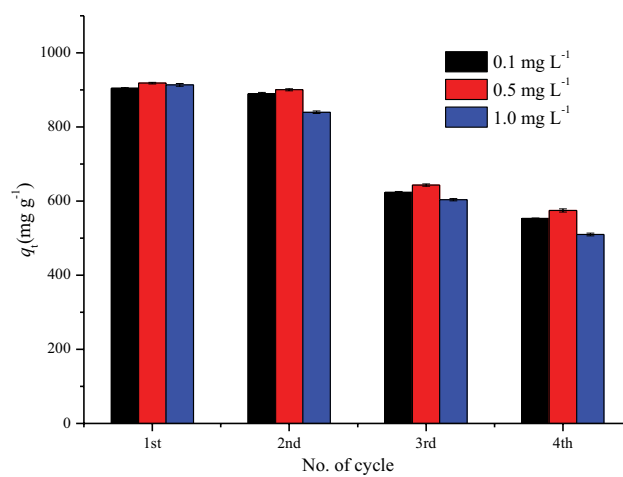

Fig. 12. Recycling of nitrogen-rich porous carbon and its application in tetracycline simulated wastewater.
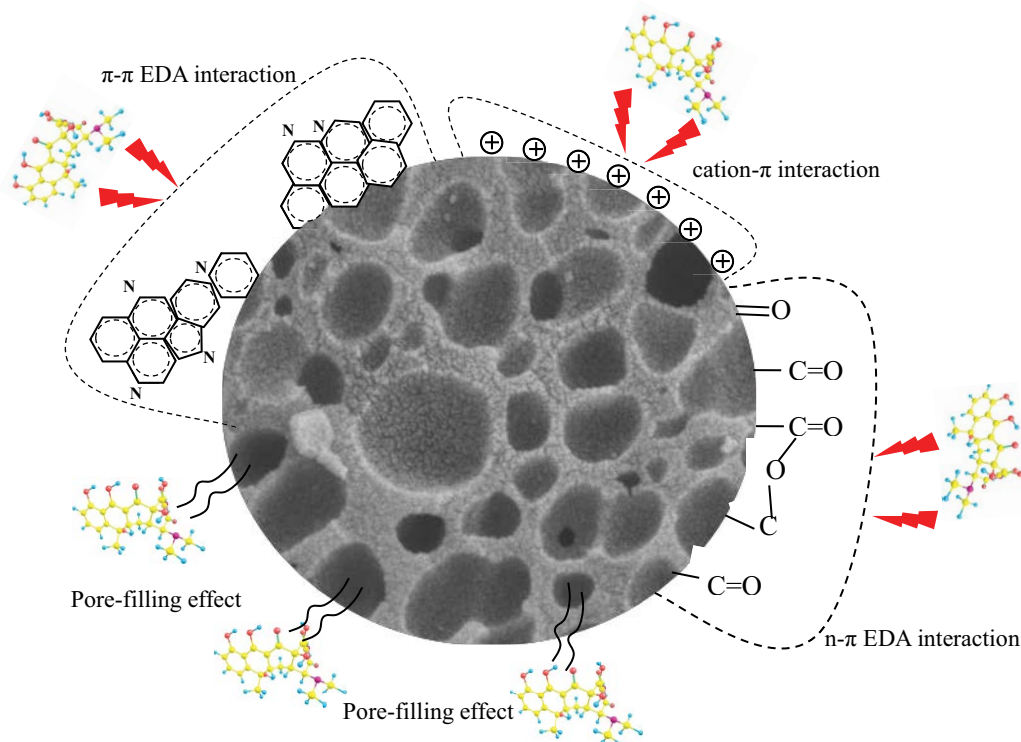

Fig. 11. Diagram of the major mechanisms for the adsorption of tetracycline by nitrogen-rich porous carbon.

3.4. Recycling and simulated wastewater applications

To investigate the economy and environmental sustainability, the waste NPC was regenerated by pyrolysis method and applied to treat the simulated wastewater with various concentrations of TC (0.1, 0.5 and 1.0 g·L^{-1}). As seen from Fig. 12, the adsorption amount (q_t) of TC on NPC initially remained unchanged at all concentrations, which might be relevant to the full exposure of active sites after regeneration. After 4 cycles, the q_t value was reduced significantly. Nonetheless, the absorbed TC by NPC still remained above 500 mg·g^{-1}. To sum up, the NPC material had good adsorption capability and recycling performance in removing TC from water.

4. Conclusion

In this research, the NPC material was successfully prepared by one-step pyrolysis and applied to remove TC from water. According to the results, the adsorption of NPC for TC was highly dependent on solution pH, contact time and initial concentration. Langmuir and pseudo-second-order models were employed to describe the adsorption behavior of NPC for TC and the maximum adsorption capability was 892.7 mg·g^{-1} at 25°C. Thermodynamic studies revealed that the adsorption process was characteristic of endothermic and spontaneous. The characterization and correlation analysis suggested that sp^2 carbon, graphitic nitrogen and carbonyl of NPC were the active sites for TC adsorption. The adsorption mechanisms mainly included pore-filling effect, π–π/n–π EDA and cation-π interactions. In conclusion, the NPC material possesses many excellent properties such as strong adsorption, good repeatability and has great application potential in TC wastewater treatment.

References

[1] H.D. Liu, G.R. Xu, G.B. Li, Preparation of porous biochar based on pharmaceutical sludge activated by NaOH and its application in the adsorption of tetracycline, J. Colloid Interface Sci., 587 (2021) 271–278.

[2] J.Y. Pan, X.T. Bai, Y.Y. Li, B.H. Yang, P.Y. Yang, F. Yu, J. Ma, HKUST-1 derived carbon adsorbents for tetracycline removal with excellent adsorption performance, Environ. Res., 205 (2022) 112425, doi: 10.1016/j.envres.2021.112425.

[3] N.M. El-Metwaly, H.A. Katouah, M.G. El-Desouky, A.A. El-Bindary, M.A. El-Bindary, Fabricating of Fe$_3$O$_4$@Ag-MOF nanocomposite and evaluating its adsorption activity for removal of doxorubicin, J. Environ. Sci. Health. Part A Toxic/Hazard. Subst. Environ. Eng., 57 (2022) 13–14.

[4] Y.Q. Shen, K. Zhu, D.D. He, J. Huang, H.M. He, L.L. Lei, W.J. Chen, Tetracycline removal via adsorption and metal-free catalysis with 3D macroscopic N-doped porous carbon nanosheets: non-radical mechanism and degradation pathway, Environ. Sci., 42 (2022) 351–366.

[5] M.C. Sun, Y.K. Ma, Y.J. Yang, X.F. Zhu, Effect of iron impregnation ratio on the properties and adsorption of KOH activated biochar for removal of tetracycline and heavy metals, Bioresour. Technol., 380 (2023) 129081, doi: 10.1016/j.biortech.2023.129081.

[6] W. Xiang, X.Y. Zhang, J.J. Chen, W.X. Zou, F. He, X. Hu, D.CW. Tsang, Y.S. Ok, B. Gao, Biochar technology in wastewater treatment: a critical review, Chemosphere, 252 (2020) 126539, doi: 10.1016/j.chemosphere.2020.126539.

[7] S.U. Masrura, P. Dissanayake, Y.Q. Sun, Y.S. Ok, D.C.W. Tsang, E. Khan, Sustainable use of biochar for resource recovery and pharmaceutical removal from human urine: a critical review, Crit. Rev. Env. Sci. Technol., 51 (2021) 3016–3048.

[8] T.A. Altalhi, M.M. Ibrahim, G.A.M. Mersal, M.H.H. Mahmoud, T. Kumeria, M.G. El-Desouky, A.A. El-Bindary, M.A. El-Bindary, Adsorption of doxorubicin hydrochloride onto thermally treated green adsorbent: equilibrium, kinetic and thermodynamic studies, J. Mol. Struct., 1263 (2022) 133160, doi: 10.1016/j.molstruc.2022.133160.

[9] F.F. Zhang, J.N. Wang, Y.J. Tian, C.X. Liu, S.Q. Zhang, L.C. Cao, Y.M. Zhou, S.C. Zhang, Effective removal of tetracycline antibiotics from water by magnetic functionalized biochar derived from rice waste, Environ. Pollut., 330 (2023) 121681, doi: 10.1016/j.envpol.2023.121681.

[10] W.L. Jiang, Y.R. Cai, D. Liu, Q.X. Shi, Q. Wang, Adsorption properties and mechanism of suaeda biochar and modified materials for tetracycline, Environ. Res., 235 (2023) 116549, doi: 10.1016/j.envres.2023.116549.

[11] Q.Y. Shi, W.B. Wang, H.M. Zhang, H.L. Bai, K.Q. Liu, J.F. Zhang, Z.H. Li, W.H. Zhu, Porous biochar derived from walnut shell as an efficient adsorbent for tetracycline removal, Bioresour. Technol., 383 (2023) 129213, doi: 10.1016/j.biortech.2023.129213.

[12] F.Z. Chen, B. Wang, G.H. Zhao, X.P. Liang, S.H. Liu, J. Liu, Optimization extraction of flavonoids from peony pods by response surface methodology, antioxidant activity and bioaccessibility *in vitro*, J. Food Meas. Charact., 17 (2023) 460–471.

[13] L.H. Xie, Z.G. Yan, M.C. Li, Y. Tian, A. Kilaru, L.X. Niu, Y.L. Zhang, Identification of phytochemical markers for quality evaluation of tree peony stamen using comprehensive HPLC-based analysis, Ind. Crops Prod., 154 (2020) 112711, doi: 10.5004/dwt.2021.27504.

[14] Q. Liu, L.B. Qu, B.Z. Ren, Effective removal of copper ions from aqueous solution by iminodiacetic acid-functionalized *Paeonia ostii* seed coats, J. Dispersion Sci. Technol., 41 (2020) 1126–1135.

[15] Q. Liu, T. Li, S.W. Zhang, L.B. Qu, B.Z. Ren, optimization and evaluation of alkali-pretreated *Paeonia ostii* seed coats as adsorbent for the removal of MB from aqueous solution, Pol. J. Chem. Technol., 20 (2018) 29–36.

[16] Q. Liu, R.P. Han, L.B. Qu, B.Z. Ren, Enhanced adsorption of copper ions by phosphoric acid-modified *Paeonia ostii* seed coats, Environ. Sci. Pollut. Res., 27 (2020) 43906–43916.

[17] S.L. Huo, X. Song, Y.B. Zhao, W. Ni, H. Wang, K.X. Li, Insight into the significant contribution of intrinsic carbon defects for the high-performance capacitive desalination of brackish water, J. Mater. Chem. A, 8 (2020) 19927–19937.

[18] H.A. Kiwaan, F.S. Mohamed, N.A. El-Ghamaz, N.M. Beshry, A.A. El-Bindary, Experimental and electrical studies of Na-X zeolite for the adsorption of different dyes, J. Mol. Liq., 42 (2021) 115877, doi: 10.1016/j.molliq.2021.115877.

[19] Y. Qin, B. Chai, C.L. Wang, J.T. Yan, G.Z. Fan, G.S. Song, New insight into remarkable tetracycline removal by enhanced graphitization of hierarchical porous carbon aerogel: performance and mechanism, Colloids Surf., A, 655 (2022) 130197, doi: 10.1016/j.colsurfa.2022.130197.

[20] Z.H. Lin, R.K. Wang, S.T. Tan, K. Zhang, Q.Q. Yin, Z.H. Zhao, P. Gao, Nitrogen-doped hydrochar prepared by biomass and nitrogen-containing wastewater for dye adsorption: effect of nitrogen source in wastewater on the adsorption performance of hydrochar, J. Environ. Manage., 334 (2023) 117503, doi: 10.1016/j.jenvman.2023.117503.

[21] C.D. Ma, J.L. Bai, X. Hu, Z.H. Jiang, L.L. Wang, Nitrogen-doped porous carbons from polyacrylonitrile fiber as effective CO$_2$ adsorbents, Environ. Sci., 125 (2023) 533–543.

[22] M.A. El-Bindary, M.G. El-Desouky, A.A. El-Bindary, Metal–organic frameworks encapsulated with an anticancer compound as drug delivery system: synthesis, characterization, antioxidant, anticancer, antibacterial, and molecular docking investigation, Appl. Organomet. Chem., 36 (2022) e6660, doi: 10.1002/aoc.6660.

[23] T. Wang, L. Xue, Y.H. Liu, L. Zhang, B.S. Xing, N self-doped hierarchically porous carbon derived from biomass as an efficient adsorbent for the removal of tetracycline antibiotics, Sci. Total Environ., 822 (2022) 153567, doi: 10.1016/j.scitotenv.2022.153567.

[24] Q.C. Wang, Y.J. Ji, Y.P. Lei, Y.B. Wang, Y.D. Wang, Y.Y. Li, S.Y. Wang, Pyridinic-N-dominated doped defective graphene as a superior oxygen electrocatalyst for ultrahigh-energy-density Zn-air batteries, ACS Energy Lett., 3 (2018) 1183–1191.

[25] J. Yang, J.D. Dai, L.L. Wang, W.N. Ge, A.T. Xie, J.S. He, Y.S. Yan, Ultrahigh adsorption of tetracycline on willow branch-derived porous carbons with tunable pore structure: isotherm, kinetics, thermodynamic and new mechanism study, J. Taiwan Inst. Chem. Eng., 96 (2019) 473–482.

[26] J. Xie, M.H. Liu, M. He, Y.F. Liu, J. Li, F.X. Yu, Ultra-efficient adsorption of diclofenac sodium on fish-scale biochar functionalized with H_3PO_4 via synergistic mechanisms, Environ. Pollut., 322 (2023) 121226, doi: 10.1016/j.envpol.2023.121226.

[27] W.H. Ding, G.L. Zhou, S.Z. Wen, J.Z. Yin, C. Liu, Y.S. Fu, L.L. Zhang, Two-dimensional activated carbon nanosheets for rapid removal of tetracycline via strong π–π electron donor receptor interactions, Bioresour. Technol., 360 (2022) 127544, doi: 10.1016/j.biortech.2022.127544.

[28] Q.H. Zhou, Y.Y. Wu, H.J. Chen, G.Y. Zhu, Y.P. Zhang, D.D. Liang, G. Chen, S.S, Tang, Preparation of *Quercus mongolica* leaf-derived porous carbon with a large specific surface area for highly effective removal of dye and antibiotic from water, Arabian J. Chem., 15 (2022) 104031, doi: 10.1016/j.arabjc.2022.104031.

[29] H.J. Wang, Q. Liu, Z.Q. Wang, R.P. Han, Adsorption of 4-chloro-2,5-dimethoxyaniline from solution in batch mode using chemical activated pyrolytic char, Desal. Water Treat., 231 (2021) 367–376.

[30] T. Wang, L. Xue, Y.H. Liu, L. Zhang, B.S. Xing, N self-doped hierarchically porous carbon derived from biomass as an efficient adsorbent for the removal of tetracycline antibiotics, Sci. Total Environ., 822 (2022) 153567, doi: 10.1016/j.scitotenv.2022.153567.

[31] J. Xu, Y. Zhang, B. Li, S.S. Fan, H.C. Xu, D.X. Guan, Improved adsorption properties of tetracycline on KOH/KMnO₄ modified biochar derived from wheat straw, Chemosphere, 296 (2022)133981, doi: 10.1016/j.chemosphere.2022.133981.

[32] B. Li, Y. Zhang, J. Xu, Y.L. Mei, S.S. Fan, H.C. Xu, Effect of carbonization methods on the properties of tea waste biochars and their application in tetracycline removal from aqueous solutions, Chemosphere, 267 (2021) 129283, doi: 10.1016/j.chemosphere.2020.129283.

[33] F.K. Mostafapour, M. Yilmaz, A.H. Mahvi, A. Younesi, F. Ganji, D. Balarak, Adsorptive removal of tetracycline from aqueous solution by surfactant-modifed zeolite: equilibrium, kinetics and thermodynamics, Desal. Water. Treat., 247 (2022) 216–228.

[34] A.D. Khatibi, A.H. Mahvi, N. Mengelizadeh, D. Balarak, Adsorption–desorption of tetracycline onto molecularly imprinted polymer: isotherm, kinetics, and thermodynamics studies, Desal. Water. Treat., 230 (2021) 240–251.

[35] D. Balarak, F.K. Mostafapour, H. Azarpira, Adsorption isotherm studies of tetracycline antibiotics from aqueous solutions by maize stalks as a cheap biosorbent, Desal. Water. Treat., 8 (2016) 16664–16675.

[36] Y.L. Mei, J. Xu, Y. Zhang, B. Li, S.S. Fan, H.C. Xu, Effect of Fe–N modification on the properties of biochars and their adsorption behavior on tetracycline removal from aqueous solution, Bioresour. Technol., 325 (2021) 124732, doi: 10.1016/j.biortech.2021.124732.

[37] J.Y. Tang, Y.F. Ma, Z.K. Deng, P. Li, X.B. Qi, Z.L. Zhang, One-pot preparation of layered double oxides-engineered biochar for the sustained removal of tetracycline in water, Bioresour. Technol., 381 (2023) 129119, doi: 10.1016/j.biortech.2023.129119.

[38] J.E. Kim, S.K. Bhatia, H.J. Song, E.J. Yoo, Y.K. Choi, Adsorptive removal of tetracycline from aqueous solution by maple leaf-derived biochar, Bioresour. Technol., 306 (2020) 123092, doi: 10.1016/j.biortech.2020.123092.

[39] Y.J. Ai, Y. Liu, Y.Z. Huo, C.F. Zhao, L. Sun, B. Han, X.R. Cao, X.K. Wang, Insights into the adsorption mechanism and dynamic behavior of tetracycline antibiotics on reduced graphene oxide (RGO) and graphene oxide (GO) materials, Environ. Sci. Nano, 6 (2019) 3336–3348.

[40] Y.Y. Wang, L.H. Xu, F. Wei, D. Tal, M. Zhang, R.L. Zhu, Insights into the adsorption mechanism of tetracycline on hierarchically porous carbon and the effect of nanoporous geometry, Chem. Eng. J., 437 (2022) 135454, doi: 10.1016/j.cej.2022.135454.

[41] A. Ejsmont, J. Goscianska, Morphology controlled nitrogen-doped mesoporous carbon vehicles for sustained release of paracetamol, Microporous Mesoporous Mater., 350 (2023) 112449, doi: 10.1016/j.micromeso.2023.112449.

[42] G. Joanna, A. Ejsmont, A. Stasiłowicz-Krzemień, S. Sip, J. Cielecka-Piontek, Enhancing antimicrobial activity of β-lactam antibiotic via functionalized mesoporous carbon-based delivery platforms, Microporous Mesoporous Mater., 343 (2022): 112160, doi: 10.1016/j.micromeso.2022.112160.

[43] G. Joanna, A. Ejsmont, A. Kubiak, D. Ludowicz, A. Stasilowicz, J. Cielecka-Piontek, Amine-grafted mesoporous carbons as benzocaine-delivery platforms, Materials, 14 (2021) 2188, doi: 10.3390/ma14092188.

[44] J.L. Liu, E. Zong, H.Y. Fu, S.R. Zheng, Z.Y. Xu, D.Q. Zhu, Adsorption of aromatic compounds on porous covalent triazine-based framework, J. Colloid Interface Sci., 372 (2012) 99–107.

[45] R.W. Newberry, R.T. Raines, The $n{\rightarrow}\pi^*$ interaction, Acc. Chem. Res., 50 (2017) 1838–1846.